RSC Advances

ROYAL SOCIETY OF CHEMISTRY

www.rsc.org/advances

RSC Advances

Dynamic Article Links ►

Cite this: DOI: 10.1039/c0xx00000x

www.rsc.org/xxxxxx

ARTICLE TYPE

Nano-Fe_3O_4 encapsulated-silica supported boron trifluoride as a novel heterogeneous solid acid for solvent-free synthesis of arylazo-1-naphthol derivatives

Abdolhamid Bamoniri* and Naimeh Moshtael-Arani

Received (in XXX, XXX) Xth XXXXXXXXX 20XX, Accepted Xth XXXXXXXXX 20XX
DOI: 10.1039/b000000x

Nano-Fe_3O_4 encapsulated-silica supported boron trifluoride (Fe_3O_4@SiO_2–BF_3) as a new type of green heterogeneous solid acid was prepared by the immobilization of $BF_3 \cdot Et_2O$ on the surface of Fe_3O_4@SiO_2 core-shell nanoparticles and characterized by Fourier transform-infrared spectroscopy (FT-IR), X-ray diffraction (XRD), vibrating sample magnetometer (VSM), field emission-scanning electron microscope (FE-SEM), energy dispersive X-ray (EDS), and transmission electron microscope (TEM). Then, this super solid acid as an acidic reagent was used for the synthesis of aryl diazonium salts as a starting reactant and following, their diazo coupling with 1-naphthol in a basic solvent-free medium at room temperature. Main advantages of this clean method were high yields, short reaction times, room temperature, no need to corrosive and toxic liquid acids and solvents. In addition, long-term stability of aryl diazonium salts supported on Fe_3O_4@SiO_2–BF_3 magnetic nanoparticles (MNPs) at room temperature was one of the most important results of this procedure.

Introduction

In recent years, solvent-free organic reactions[1] have captured great interest because of their many advantages such as high efficiency and selectivity, easy separation and purification, mild reaction condition, reduction in waste, simplicity in progress and handling, and benefit to the industry as well as the environment. Aromatic azo compounds constitute a very important class of organic dyes because of their widespread applications in many areas of technology and medicine. They are well known for their use as colorants in the textile industries,[2] digital printing and photography.[3] They are also applied as chiral receptors,[4] liquid crystals,[5] new glassy materials,[6] chiral switches in photochemistry,[7] dyes for drug, food, cosmetic, biomedicine,[8] and molecular recognition.[9] As synthesis of azo dyes requires some special conditions such as low temperature and concentrated liquid acid, in addition to high costs, it leads to corrosion of reactors and equipments, too.[10] Nowadays, solid supported reagents have resolved these problems and improved activity and selectivity rather than individual reagents.[11] Such reagents not only simplify purification processes but they also help prevent release of reaction residues into the environment.[12] In this regard, nano structure solid acids exhibit higher activity and selectivity than their corresponding bulk materials due to their particular physical and chemical properties especially large surface to volume ratio.[13] Recently, Fe_3O_4 MNPs has appeared as a new kind of efficient catalyst support due to low toxicity, ease of surface modification, unique physical properties including the high surface area and superparamagnetism.[14] In order to prevent the aggregation of Fe_3O_4 nanoparticles, its surface is usually modified with silica layer, taking advantage of being biocompatible and hydrophilic and, also, because the surface silanol groups can easily react with various organic and inorganic materials to achieve the certain purposes especially in the field of catalysis.[15] As a continuation of our efforts on the development of heterogeneous solid acids in organic transformations,[16] we herein report the preparation and characterization of a novel and eco-friendly magnetic solid acid as Fe_3O_4@SiO_2–BF_3 and its utility for the synthesis of arylazo-1-naphthol dyes in a solvent-free environment at room temperature. In this method, it is not require providing special cold condition for stabilization of aryl diazonium salt. The reaction easily takes place at room temperature and resulting diazonium salt can remain on the solid substrate for several months. To the best of our knowledge, this research is the first report about long-term stability of aryl diazonium salts supported on the surface of MNPs and their use as the reactant for synthesis of arylazo-1-naphthols in solvent-free condition. The findings of this research may have implications for effective synthesis on a larger scale in dyeing and medical industries.

Results and discussion

This research was performed in three stages. Initially, Fe_3O_4@SiO_2–BF_3 MNPs was synthesized and identified by FT-IR, XRD, VSM, FE-SEM, EDS, and TEM. In the second stage, aryl diazonium salts were synthesized in the presence of Fe_3O_4@SiO_2–BF_3 nanoparticles at room temperature and their structure and stability was investigated. The third stage was diazo coupling of aryl diazonium salts supported on Fe_3O_4@SiO_2–BF_3 with basic 1-naphthol under solvent-free grinding condition.

Synthesis and characterization of Fe_3O_4@SiO_2–BF_3 nanoparticles

Fe_3O_4@SiO_2–BF_3 core–shell nanoparticles, with Fe_3O_4 spheres as the core and silica supported BF_3 as the shell, was prepared by a simple and convenient method. At first, Fe_3O_4 nanoparticles were prepared by chemical co-precipitation of $FeCl_2 \cdot 4H_2O$ and $FeCl_3 \cdot 6H_2O$ in ammonium hydroxide solution. To improve the chemical stability of Fe_3O_4 and prevent self-aggregation, its surface engineering was successfully performed by the suitable deposition of SiO_2 onto Fe_3O_4 surface via the ammonia-catalyzed hydrolysis of tetraethylorthosilicate (TEOS). Next, the Fe_3O_4@SiO_2 spheres served as support for the immobilization of BF_3 groups by simple stirring of Fe_3O_4@SiO_2 and $BF_3 \cdot Et_2O$ in ethanol. All three steps were carried out under sonication condition at room temperature (Scheme 1).

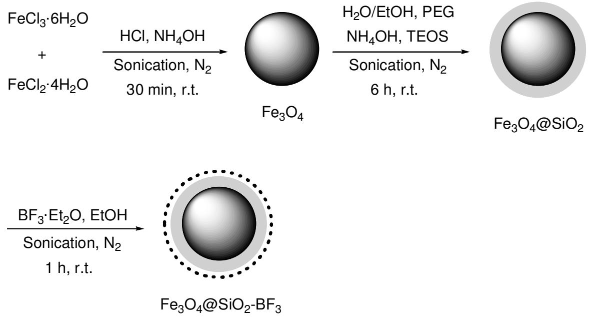

Scheme 1 Preparation of Fe_3O_4@SiO_2–BF_3 MNPs under sonication condition at room temperature.

In order to identify the molecular structures of Fe_3O_4, Fe_3O_4@SiO_2, and Fe_3O_4@SiO_2–BF_3 MNPs, FT-IR analysis of three mentioned samples was performed (Fig. 1). Fe_3O_4 was identified by a stretching vibration of the Fe–O absorption peak at 576 cm^{-1}, O–H stretching vibration at 3429 cm^{-1} and O–H deformed vibration at 1625 cm^{-1} in Fig. 1a. The FT-IR spectrum of Fe_3O_4@SiO_2 (Fig. 1b) displayed characteristic peaks at 1093 and 800 cm^{-1} corresponding to symmetrical and asymmetrical vibrations of Si–O–Si, respectively. Weak band at 466 cm^{-1} corresponded to the Si–O–Fe stretching vibrations of the Fe_3O_4@SiO_2 core-shell, overall confirming the presence of SiO_2 in the sample. The successful covalent linking of the $BF_3 \cdot Et_2O$ on the surface of Fe_3O_4@SiO_2 core-shell was proved by the appearance of a new band at 1457 cm^{-1}, which originates from the absorption of B–O (Fig. 1c). The absorption band of B–F was hidden under Si–O band. Also, the ethanolic OH and existing moisture in $BF_3 \cdot Et_2O$ caused a broad O–H stretching band at wavenumber of 3221 cm^{-1}. Again observation of Fe_3O_4 absorption peaks in Fig. 1b and Fig. 1c implies that Fe_3O_4 MNPs do not change chemically or physically after coating and surface modification processes. According to this information and regarding the reported structure of $BF_3 \cdot SiO_2$ in the literature,[17] the final structure of nano Fe_3O_4@SiO_2–BF_3 was predicted in Scheme 2.

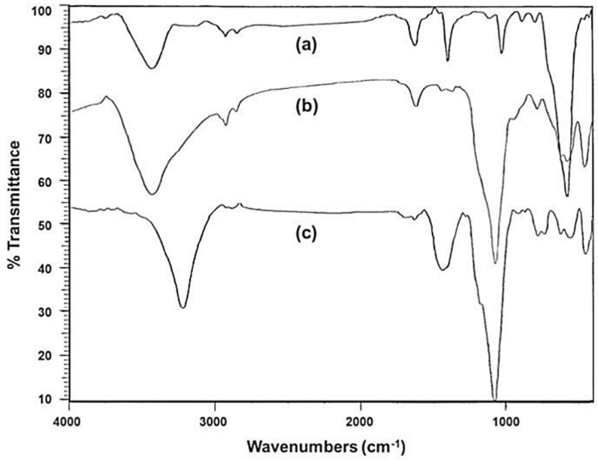

Fig. 1 FT-IR spectra of a) Fe_3O_4, (b) Fe_3O_4@SiO_2 and (c) Fe_3O_4@SiO_2–BF_3.

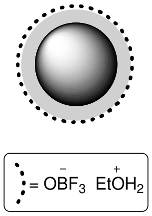

Scheme 2 The structure of Fe_3O_4@SiO_2–BF_3 MNPs.

Fig. 2 shows the XRD powder diffraction patterns of three synthesized MNPs. The data for the Fe_3O_4 nanoparticles at 2θ of 30.22, 35.61, 43.25, 53.58, 57.30, 62.89, and 74.66° (Fig. 2a) corresponded to the standard Fe_3O_4 powder diffraction data. Moreover, the relatively sharp peaks observed indicate phase purity of Fe_3O_4 nanoparticles, which are consistent with the presence of the cubic inverse spinel structure of Fe_3O_4. The XRD pattern of the Fe_3O_4@SiO_2 (Fig. 2b) was in good agreement with that of Fe_3O_4 phase, except for a broad peak around 2θ of 20-30° corresponding to amorphous phase of SiO_2. This indicates that the MNPs obtained after the coating process are composed of Fe_3O_4 core and amorphous SiO_2 shell. The XRD pattern of the modified Fe_3O_4@SiO_2 with $BF_3 \cdot Et_2O$ in Fig. 2c was nearly the same with Fig. 2b, which it seems that the surface modification by BF_3 group has little effect on the XRD pattern of Fe_3O_4@SiO_2 nanoparticles, because of the shielding effect of Fe_3O_4 and SiO_2 peaks. However, the changes in peaks intensity in spectra 2b and 2c and increase the noise in Fig. 2c can verify the linking of BF_3 on the surface of Fe_3O_4@SiO_2 core-shell MNPs. Furthermore, characteristic peaks of Fe_3O_4 were observed in three samples, thereby indicating that the binding process did not induce any phase change.

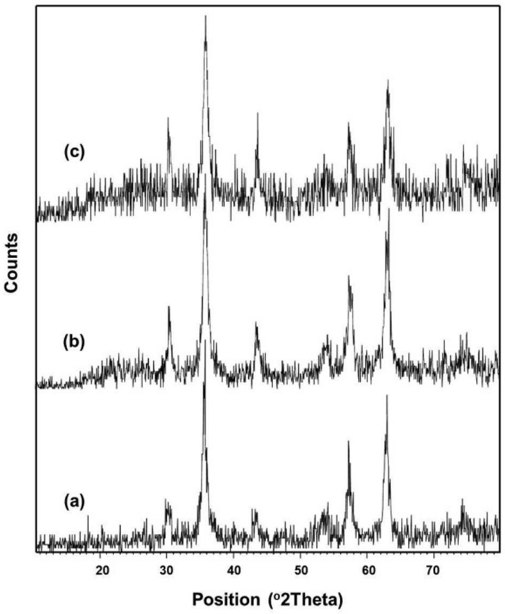

Fig. 2 XRD patterns of (a) Fe_3O_4, (b) $Fe_3O_4@SiO_2$, and (c) $Fe_3O_4@SiO_2–BF_3$.

The magnetic properties of synthesized Fe_3O_4, $Fe_3O_4@SiO_2$, and $Fe_3O_4@SiO_2–BF_3$ nanoparticles were assessed by VSM at room temperature. The magnetization curve in Fig. 3 indicates magnetization as a function of applied magnetic field. The saturation magnetization of the $Fe_3O_4@SiO_2$ nanoparticles in Fig. 3b was about 29.15 emu/g, and this reduced to 27.44 emu/g after supporting with $BF_3{\cdot}Et_2O$ (Fig. 3c). Both of these values were much lower than the initial saturation magnetization of Fe_3O_4 nanoparticles (59.2 emu/g) in Fig. 3a. The decrease of the saturation magnetization after surface coating of Fe_3O_4 confirms the presence of a diamagnetic outer shell (SiO_2 or $SiO_2–BF_3$) at the surface of the Fe_3O_4 particles.

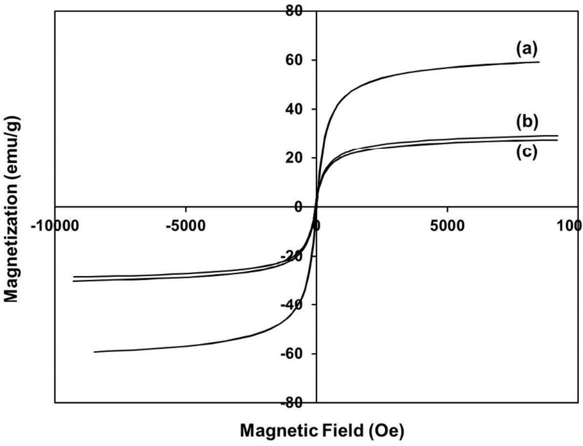

Fig. 3 Magnetization curves of (a) Fe_3O_4, (b) $Fe_3O_4@SiO_2$, and (c) $Fe_3O_4@SiO_2–BF_3$.

The high magnification FE-SEM images of the purified MNPs are displayed in Fig. 4(a-c). These images clearly showed the surface morphology of three kinds of synthesized MNPs with a nearly spherical shape. Elemental components of three MNPs were characterized by EDS analysis. Fig. 4d shows EDS of the Fe_3O_4 nanoparticles, in which the particles contain Fe and O elements. The presence of Fe, O and Si elements in Fig. 4e verified the coating of Fe_3O_4 core by SiO_2 shell. The appearance of two new signals related to F and C elements in Fig. 4f confirmed supporting of $BF_3{\cdot}Et_2O$ on $Fe_3O_4@SiO_2$ core-shell nanoparticles according to Scheme 2.

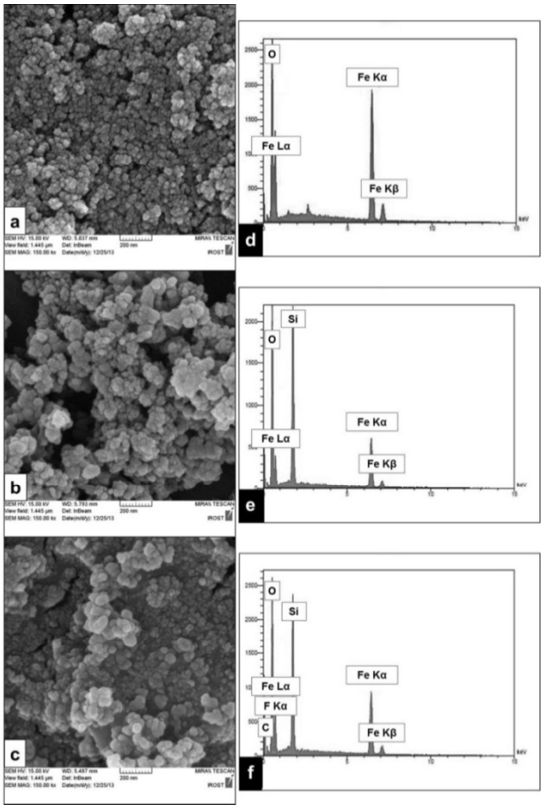

Fig. 4 FE-SEM images of (a) Fe_3O_4, (b) $Fe_3O_4@SiO_2$, (c) $Fe_3O_4@SiO_2–BF_3$ and EDS spectra of (d) Fe_3O_4, (e) $Fe_3O_4@SiO_2$, (f) $Fe_3O_4@SiO_2–BF_3$.

TEM images of Fe_3O_4 and $Fe_3O_4@SiO_2–BF_3$ are displayed in Fig. 5. As demonstrated in Fig. 5a, Fe_3O_4 nanoparticles have the spherical morphology. In Fig. 5b, two regions with different electron densities can be distinguished that confirms the Fe_3O_4 nanoparticles were successfully coated with a thin layer of a different phase. However, it can be observed that the sample is nearly in core-shell structure. An electron dense region (black colour) which corresponds to Fe_3O_4 cores and a less dense or more translucent region (ash colour) surrounding these cores that is $SiO_2–BF_3$ shell. From the size distribution histograms, the average size of 9 nm for Fe_3O_4 and 13 nm for $Fe_3O_4@SiO_2–BF_3$ nanoparticles could be estimated.

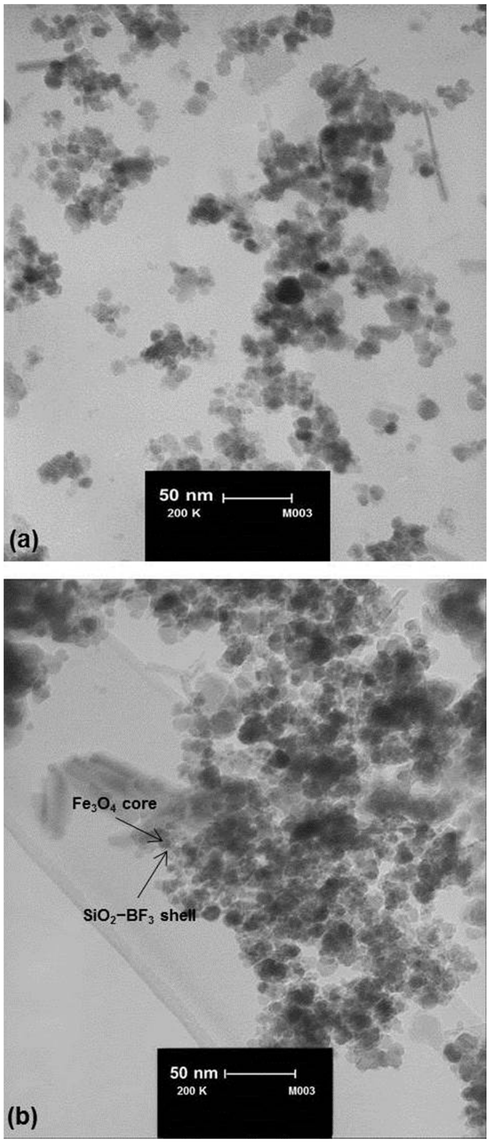

Fig. 5 TEM images of (a) Fe_3O_4, and (b) $Fe_3O_4@SiO_2–BF_3$ nanoparticles.

Finally, $Fe_3O_4@SiO_2–BF_3$ was identified by using the techniques described above, and applied for synthesis of arylazo-1-naphthol derivatives.

Synthesis and characterization of aryl diazonium salts

Aryl diazonium salts are usually synthesized in the presence of a liquid acid dissolved in water at low temperatures between 0 to 5 °C, because temperatures above 5 °C generally promote phenol formation in aqueous media. Thus, as synthesis of aryl diazonium salts has limitations and drawbacks such as the control and maintenance of the low-temperature, using toxic liquid acids that are incompatible with environment, and most important of all, instability of aryl diazonium salts at room temperature, we tried to resolve these problems by the development a green and simple procedure for synthesis of aryl diazonium salts and in continue, their diazo coupling with 1-naphthol.

At first, in order to evaluate the efficiency of $Fe_3O_4@SiO_2–BF_3$ MNPs in diazotization reaction, an initial optimization of the kind and amount of acidic reagent was performed via diazotization of 4-chloro aniline as a model substrate. A range of parameters such as stability of 4-chlorophenyl diazonium salt at room temperature, reaction time of diazotization, and yield of resulted 4-chlorophenylazo-1-naphthol were screened in Table 1.

Solid acids such as silica phosphoric acid and silica chloride gave the 4-chlorophenylazo-1-naphthol with modest yields of 57% and 61%, respectively (Table 1, entries 1 and 2). The stability of aryl diazonium salt supported on above mentioned solid acids was maximum 2 days. $Fe_3O_4@SiO_2$ and $BF_3·Et_2O$ sources were also tested individually. There was no reaction in the presence of neither $Fe_3O_4@SiO_2$ nor $BF_3·Et_2O$ (Table 1, entries 3 and 4), while $Fe_3O_4@SiO_2–BF_3$ with different loadings afforded the improved yields from 87% to 95% for 4-chlorophenylazo-1-naphthol (Table 1, entries 5-8). These results clearly indicated that the presence of Brönsted acid sites on the solid acid surface is essential for promoting diazotization. Also, the rate of diazotization in the presence of $Fe_3O_4@SiO_2–BF_3$ MNPs was much higher than silica phosphoric acid and silica chloride.

In another comparative study (Table 1, entries 5-8), the effect of $Fe_3O_4@SiO_2$ loading by $BF_3·Et_2O$ on the acidic performance of $Fe_3O_4@SiO_2–BF_3$ was investigated. Although the time of diazotization and the stability of aryl diazonium salt supported on $Fe_3O_4@SiO_2–BF_3$ nanoparticles with different loadings in the same conditions were approximately identical, but 10 wt% $Fe_3O_4@SiO_2–BF_3$ resulted in the highest yield of the corresponding azo dye (Table 1, entry 6). In conclusion, 10 wt% $Fe_3O_4@SiO_2–BF_3$ was selected as the most ideal acid for synthesis of arylazo-1-naphthol dyes among those listed in Table 1.

In addition, with more investigations, it was found that aryl diazonium salts supported on $Fe_3O_4@SiO_2–BF_3$ nanoparticles underwent no significant change at room temperature for several months. To explore the reason of this unusual stability, FT-IR spectrum of 4-chlorophenyl diazonium salt was studied (Fig. 6).

Table 1 Comparison of efficiency of various acids in synthesis of 4-chlorophenyl diazonium salt.

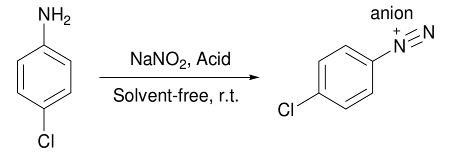

Entry	Acid (wt %)	Stability at r.t.	Time of diazotization	Yield[a] (%)
1	SPA[b] (10)	~ 2 days	35 min	57
2	SC[c] (10)	~ 2 days	30 min	61
3	$Fe_3O_4@SiO_2$	----	No reaction	---
4	$BF_3·Et_2O$	----	No reaction	---
5	$Fe_3O_4@SiO_2–BF_3$ (5)	> 13 months	12 sec	89
6	$Fe_3O_4@SiO_2–BF_3$ (10)	> 13 months	6 sec	95
7	$Fe_3O_4@SiO_2–BF_3$ (15)	> 13 months	8 sec	90
8	$Fe_3O_4@SiO_2–BF_3$ (20)	> 13 months	8 sec	87

[a] The yields refer to the total isolated yield of 2-(4-chlorophenylazo)-1-naphthol and 4-(4-chlorophenylazo)-1-naphthol after adding fresh 4-chlorophenyl diazonium salt into basic 1-naphthol. [b] Silica phosphoric acid. [c] Silica chloride.

In this spectrum, the ethanolic OH and existing moisture in $BF_3 \cdot Et_2O$ caused a broad O–H stretching band at wavenumber of 3419 cm^{-1}. The appearance of a new band at 2289 cm^{-1} clearly demonstrated N≡N stretching vibration and verified the formation of 4-chlorophenyl diazonium salt. The absorption bands of B–O and Si–O vibrations were observed at 1442 and 1085 cm^{-1}, respectively. Aromatic C–H bending vibrations, C–Cl and Fe–O stretching bands were revealed at 829, 634, and 586 cm^{-1}, respectively.

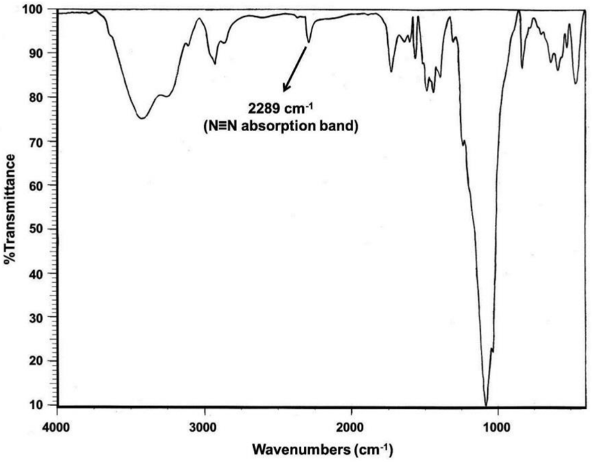

Fig. 6 FT-IR spectrum of 4-chlorophenyl diazonium salt supported on $Fe_3O_4@SiO_2–BF_3$ MNPs.

According to this information, the structure of aryl diazonium salts supported on MNPs was guessed. Scheme 3 reveals that in this probable structure, aryl diazonium cations are located on the surface of negatively charged particles called Fe_3O_4–silica trifluoroborate nanoparticles. So, the presence of bulky anions and charge–charge interactions between nitrogen and boron atoms are the possible reasons of unusual stability of these salts.

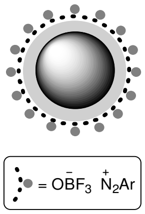

Scheme 3 The probable structure of aryl diazonium salt supported on $Fe_3O_4@SiO_2–BF_3$ nanoparticles.

As a result, the high conversions of aniline derivatives to aryl diazonium salts and their long-term stability showed that the $Fe_3O_4@SiO_2–BF_3$ has strong and sufficient acidic sites, which are responsible for excellent performance in synthesis of aryl diazonium salts.

After optimization of the conditions, aniline derivatives including electron-withdrawing and electron-donating substituents were ground with $NaNO_2$ and $Fe_3O_4@SiO_2–BF_3$ nanoparticles. Aryl diazonium salts were obtained in a very short time with an excellent conversion at room temperature (Scheme 4). Indeed, due to the high acidic strength of $Fe_3O_4@SiO_2–BF_3$ nanoparticles, the reaction was done so rapid that the substituent type could not effect on the time of diazotization.

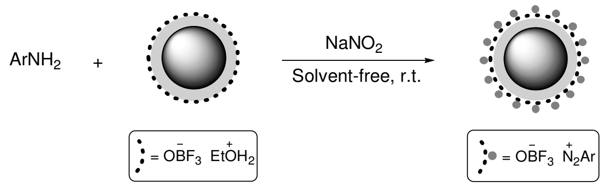

Scheme 4 Diazotization of aromatic amines in the presence of $Fe_3O_4@SiO_2–BF_3$ nanoparticles.

It is important to note that $Fe_3O_4@SiO_2–BF_3$ in diazotization reaction acts as a two-function reagent, so that, on one side, its acidic protons convert the nitrite anions (NO_2^-) in $NaNO_2$ to nitrosonium cations (NO^+) to promote diazotization and on the other side, its bulky anions cause the stability of aryl diazonium cations.

Synthesis of arylazo-1-naphthol dyes

The most common synthetic route to the arylazo-1-naphthol compounds involves coupling of aryl diazonium salts with 1-naphthol in basic solution. Although using of water for preparation of 1-naphthoxide salt seems to be necessary, but like the previous step, using of water cause the formation of some phenoxide salt and its attack to diazonium salt to form phenolic azo dyes. To prevent this problem, the reaction was performed under solvent-free condition toward green chemistry. So, we ground solid 1-naphthol with some NaOH in a mortar. The moisture absorbed by the reaction mixture during the grinding seems to be sufficient for the formation of a homogeneous mixture. Moreover, the higher concentration of reactants in the absence of solvent at room temperature usually leads to more favourable kinetics than in solution.[18]

In this reaction, diazo coupling of aryl diazonium salts with 1-naphtoxide led to two products in which 4-arylazo-1-naphthol derivatives were the major products and 2-arylazo-1-naphthol derivatives got as the minor products. The resulted two main products were easily separated by flash column chromatography and identified by ^1H-NMR and FT-IR spectroscopic methods. The molar ratios of these two dyes were determined from integral intensities of OH/NH signals in ^1H-NMR spectrum (ratio 5:1 for 4-arylazo-1-naphthol to 2-arylazo-1-naphthol). Total yields of two products are shown in Table 2.

It is also important that the electronic effects of aryl diazonium salt substituents do not play significant role in the rate of diazo coupling step. However, coupling reaction occurred rapidly regardless of substituent effects.

Totally, in this research we investigated the application of $Fe_3O_4@SiO_2–BF_3$ MNPs as a strong and useful solid acid reagent for synthesis of azo dyes based on 1-naphthol via a green procedure.

Table 2 Solvent-free synthesis of arylazo-1-naphthol derivatives at room temperature.

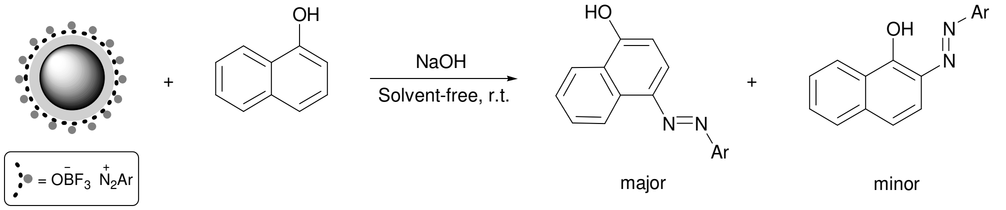

Entry	Amine	2-Arylazo-1-naphthol (a′)	4-Arylazo-1-naphthol (b′)	Yield[a] (%)	MP$_{\text{found (Lit.) in a′/ found (Lit.) in b′}}$ (°C)
1	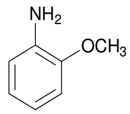	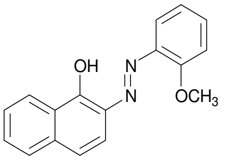	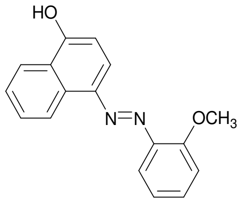	92	181-183 (180.5-181)[19]/ 176-178 (177-178)[20]
2	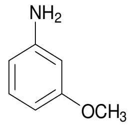	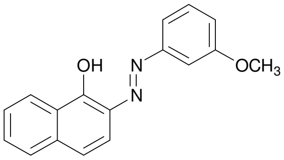	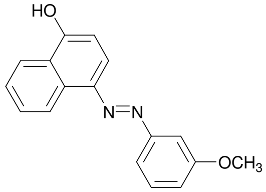	89	116-118/ 157-159 (159)[20]
3	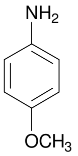	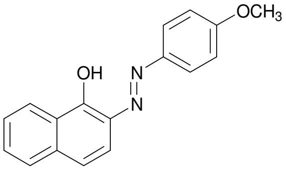	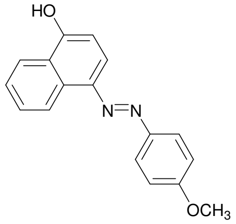	93	127-129 (127.5–128)[19]/ 173-175 (173)[20]
4	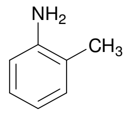	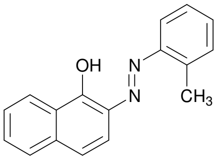	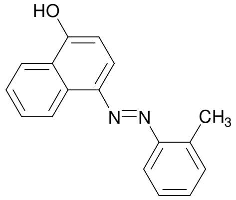	91	157-159 (156)[19]/ 160-162 (162-163)[20]
5	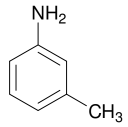	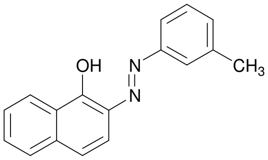	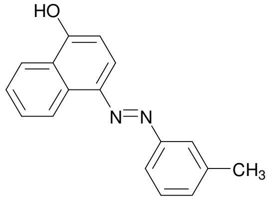	90	116-118 (117-118)[21]/ 201-203 (200)[20]
6	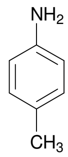	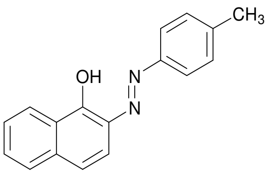	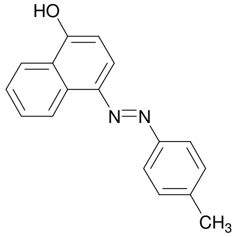	96	148-150 (151)[19]/ 211-213 (211.5)[20]

7	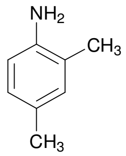	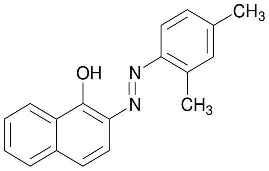	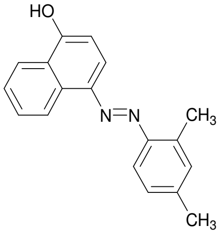	87	184-186 (186)[21]/ 138-140
8	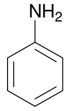	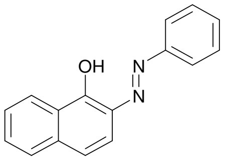	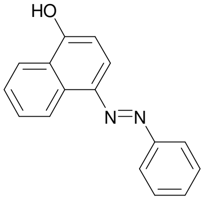	89	137-139 (138)[22]/ 207-209 (208)[20]
9	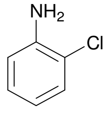	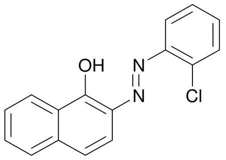	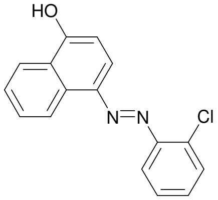	92	172-174/ 188-190 (189.5-190.5)[20]
10	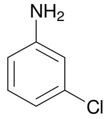	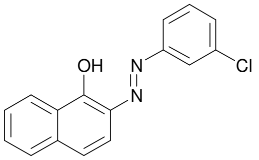	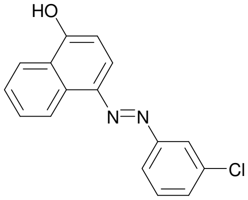	90	152-154/ 228-230 (227.5-228)[20]
11	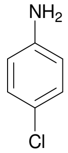	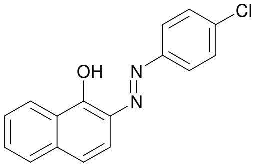	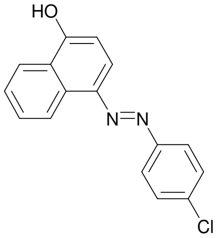	95	187-189 (187)[21]/ 229-231 (229.5)[20]
12	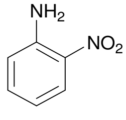	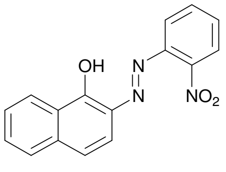	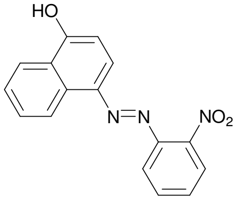	85	216-218 (216)[23]/ 258-260 (256-257)[20]

[a] Total isolated yield of 2-arylazo-1-naphthols and 4-arylazo-1-naphthols after chromatography.

Experimental

Materials and apparatus

Chemicals and solvents were purchased from Merck and Sigma-Aldrich Companies. Melting points were obtained with a micro melting point apparatus (Electrothermal, Mk3) and are uncorrected. ^{1}H-NMR spectra were recorded on a Bruker DRX-400 Avance spectrometer. Tetramethyl silane (TMS) was used as an internal reference and $CDCl_3$ and DMSO-d_6 used as solvents. FT-IR spectra were run on a Nicolet Magna 550 spectrometer. The ultrasonic equipment used for the synthesis of MNPs (Fe_3O_4, Fe_3O_4@SiO_2, and Fe_3O_4@SiO_2–BF_3) was a *Sonica 2200ETH S3 SOLTEC* ultrasonic bath (Italy) with a working frequency of 40 KHz. XRD patterns were acquired using a Philips Xpert MPD diffractometer equipped with a Cu Kα anode (λ=1.54 Å) in the 2θ range from 10 to 80°. Magnetization of the samples was recorded as a function of the applied magnetic field sweeping between ±10 kOe at room temperature. All measurements were performed on a vibrating sample magnetometer device (Meghnatis Daghigh Kavir Co.; Kashan Kavir; Iran). The morphology of the synthesized samples was studied by a Mira II LMU Tescan FE-SEM made in Czech Republic. Elemental composition of three above mentioned MNPs was investigated by EDS spectroscopy (SAMX, France). The average size of Fe_3O_4 and Fe_3O_4@SiO_2–BF_3 MNPs was analyzed by TEM using a Philips CM120 with a LaB6 cathode and accelerating voltage of 120 kV.

Synthesis of $Fe_3O_4@SiO_2–BF_3$ MNPs

The synthesis of Fe_3O_4 nanoparticles was carried out according to the known procedure using chemical co-precipitation method by a little modification of the methodology already reported in the literature.[24] Briefly, $FeCl_3·6H_2O$ (8.0 g, 0.0216 mol) and $FeCl_2·4H_2O$ (3.5 g, 0.0108 mol) with molar ratio of 1:2, were dissolved in 38 mL of deoxygenated 0.4 M HCl solution. Then, 375 mL of deoxygenated 0.7 M ammonia solution was quickly added into the reaction mixture under sonication and nitrogen atmosphere. This resulted in immediate formation of a black precipitate of Fe_3O_4 (magnetite). The sonication of magnetite dispersion was continued for 30 min. Finally, the precipitates were collected using an external magnetic field and washed for several times with distilled water and ethanol. The synthesized Fe_3O_4 MNPs were suspended in 50 mL of distilled water for use in the next steps.

Modified Stöber sol-gel process,[25] was used for coating magnetite nanoparticles with a silica shell. Typically, 50 mL of magnetite suspended in water was added to 250 mL ethanol and sonicated at room temperature for 20 min under nitrogen flow. Then 11.85 mL PEG 200, 50 mL distilled water, 25 mL NH_3 (28%) were added respectively, and after 15 min, 5 mL of TEOS was introduced into the suspension and the mixture was again sonicated for 6 h. $Fe_3O_4@SiO_2$ nanoparticles was centrifuged at 3000 rpm for 10 min, the solvent was discarded and nanoparticles were washed three times with water and then ethanol and dried in vacuum at room temperature.

In the final stage, $BF_3·Et_2O$ (0.45 mL) was added drop-wise to a slurry containing $Fe_3O_4@SiO_2$ core-shell nanoparticles (4.5 g) and ethanol (15 mL). The mixture was sonicated for 1 h at room temperature. The resulted suspension was filtered and dried at room temperature to obtain the brown solid named nano $Fe_3O_4@SiO_2–BF_3$ (10 wt%).

Typical procedure for synthesis of arylazo-1-naphthol dyes

For synthesis of arylazo-1-naphthol derivatives, we mixed aromatic amines (2 mmol) with sodium nitrite (3 mmol) and $Fe_3O_4@SiO_2–BF_3$ nanoparticles (0.3 gr), respectively in a mortar with a pestle by rapid grinding. The progress of reaction was monitored by TLC (Ethyl acetate/n-Hexane). On the other side, for preparation of 1-naphtoxide salt, we ground 2 mmol of 1-naphthol and 10 mmol NaOH in the other mortar. Then, aryl diazonium salt was added to 1-naphthoxide salt and mixing and grinding resumed for a short time (about 3 min). After the completion of reaction and formation of two main products (2-arylazo-1-naphthol and 4-arylazo-1-naphthol), the mixture was washed by distilled water (3×10 mL) and then by acetone (4×5 mL). Two final products were separated by flash column chromatography with silica mesh of 230-400 (40-63 µm).

Conclusion

$Fe_3O_4@SiO_2–BF_3$ MNPs as a novel heterogeneous solid acid reagent was prepared by supporting of $BF_3·Et_2O$ on the surface of $Fe_3O_4@SiO_2$ core-shell nanoparticles and characterized by various methods. Then, some brilliant arylazo-1-naphthol derivatives were successfully synthesized by diazotization of aniline derivatives in the presence of $Fe_3O_4@SiO_2–BF_3$ MNPs and their diazo coupling with 1-naphthol at room temperature. Using $Fe_3O_4@SiO_2–BF_3$ and solvent-free procedure caused the experimental simplicity, no use of special conditions such as liquid acids and low temperature, compatibility with environment, efficient yields, short reaction times and made this procedure attractive to synthesize a variety of these important dyes. The structure and stability of aryl diazonium salt supported on $Fe_3O_4@SiO_2–BF_3$ MNPs were studied, too.

Acknowledgments

The authors are grateful to University of Kashan for supporting this work by Grant No. 159189/41.

Notes and references

Department of Organic Chemistry, Faculty of Chemistry, University of Kashan, Kashan 87317-51167, Iran.
E-mail: bamoniri@kashanu.ac.ir

1 (a) T. Kaicharla, S. R. Yetra, T. Roy and A. T. Biju, *Green Chem.*, 2013, **15**, 1608–1614; (b) M. V. Reddy and Y. T. Jeong, *Tetrahedron Lett.*, 2013, **54**, 3546–3549; (c) M. Özil and M. Canpolat, *Polyhedron*, 2013, **51**, 82–89; (d) Z. N. Siddiqui and T. Khan, *RSC Adv.*, 2014, **4**, 2526–2537; (e) J. Kamalraja and P. T. Perumal, *Tetrahedron Lett.*, 2014, **55**, 3561–3564; (f) D. Lanari, O. Rosati and M. Curini, *Tetrahedron Lett.*, 2014, **55**, 1752–1755.

2 H. S. Freeman and A. T. Peters, Colorants for Non-Textile Applications, Elsevier Science B.V., Amsterdam, 2000.

3 P. Gregory, High Technology Applications of Organic Colorants, Plenum, New York, 1991, Chapter 9.

4 Y. Kubo, S. Maeda, S. Tokita and M. Kubo, *Nature*, 1996, **382**, 522–524.

5 R. Steinsträsser and L. Pohl, *Angew. Chem., Int. Ed.*, 1973, **12**, 617–630.

6 Y. He, X. Gu, M. Guo and X. Wang, *Opt. Mater.*, 2008, **31**, 18–27.

7 S. Pieraccini, S. Masiero, G. P. Spada and G. Gottarelli, *Chem. Commun.*, 2003, **9**, 598–599.

8 M. Tatsuta and T. Kitao, Reagent for Detecting and Diagnosing Cancer, Publication No. JP 01-207247 A, 1989.

9 A. Aszalos, J. L. Weaver and P. S. Pine, Methods of Using Azo Dyes and Their Derivatives, US Patent No. 5,468,469, 1995.

10 R. M. Christie, Colour Chemistry, Royal Society of Chemistry, Cambridge, 2001, Chapter 3.

11 (a) A. B. Atar and Y. T. Jeong, *Tetrahedron Lett.*, 2013, **54**, 1302–1306; (b) F. Jing, B. Katryniok, E. Bordes-Richard and S. Paul, *Catal. Today*, 2013, **203**, 32–39; (c) Y. B. Huang and Y. Fu, *Green Chem.*, 2013, **15**, 1095–1111; (d) M. Billamboz, F. Mangin, N. Drillaud, C. Chevrin-Villette, E. Banaszak-Léonard and C. Len, *J. Org. Chem.*, 2014, **79**, 493–500; (e) C. Battilocchio, J. M. Hawkins and S. V. Ley, *Org. Lett.*, 2014, **16**, 1060–1063; (f) K. M. Hello, H. R. Hasan, M. H. Sauodi and P. Morgen, *Appl. Catal., A*, 2014, **475**, 226–234; (g) J. G. Hernández-Cortez, M. Manríquez, L. Lartundo-Rojas and E. López-Salinas, *Catal. Today*, 2014, **220-222**, 32–38.

12 (a) J. H. Clark, Catalysis of Organic Reactions by Supported Inorganic Reagents, VCH, New York, 1994; (b) T. Okuhara, *Chem. Rev.*, 2002, **102**, 3641–3666.

13 (a) A. K. Shah, K. J. Prathap, M. Kumar, S. H. R. Abdi, R. I. Kureshy, N. H. Khan and H. C. Bajaj, *Appl. Catal., A*, 2014, **469**, 442–450; (b) M. Korzec, P. Bartczak, A. Niemczyk, J. Szade, M. Kapkowski, P. Zenderowska, K. Balin, J. Lelatko and J. Polanski, *J. Catal.*, 2014, **313**, 1–8; (c) Z. Dong, X. Le, X. Li, W. Zhang, C. Dong and J. Ma, *Appl. Catal., B*, 2014,

158-159, 129–135; (d) X. Le, Z. Dong, W. Zhang, X. Li and J. Ma, *J. Mol. Catal. A: Chem.*, 2014, **395**, 58–65; (e) T. R. Mandlimath, B. Umamahesh and K. I. Sathiyanarayanan, *J. Mol. Catal. A: Chem.*, 2014, **391**, 198–207.

14 L. H. Reddy, J. L. Arias, J. Nicolas and P. Couvreur, *Chem. Rev.*, 2012, **112**, 5818–5878.

15 (a) Y. H. Liu, J. Deng, J. W. Gao and Z. H. Zhang, *Adv. Synth. Catal.*, 2012, **354**, 441–447; (b) X. Zhang, X. He, L. Chen and Y. Zhang, *J. Mater. Chem.*, 2012, **22**, 16520–16526; (c) X. Jin, K. Zhang, J. Sun, J. Wang, Z. Dong and R. Li, *Catal. Commun.*, 2012, **26**, 199–203; (d) H. J. Xu, X. Wan, Y. Y. Shen, S. Xu and Y. S. Feng, *Org. Lett.*, 2012, **14**, 1210–1213; (e) G. M. Ucoski, F. S. Nunes, G. F. Silva, Y. M. Idemori and S. Nakagaki, *Appl. Catal., A*, 2013, **459**, 121–130; (f) F. Nemati, R. Saeedirad, *Chin. Chem. Lett.*, 2013, **24**, 370–372; (g) S. Wang, Z. Zhang, B. Liu and J. Li, *Catal. Sci. Technol.*, 2013, **3**, 2104–2112; (h) M. R. Nabid, Y. Bide and M. Niknezhad, *ChemCatChem*, 2014, **6**, 538–546; (i) F. Zhang, M. Chen, X. Wu, W. Wang and H. Li, *J. Mater. Chem. A*, 2014, **2**, 484–491; (j) R. K. Sharma, Y. Monga and A. Puri, *J. Mol. Catal. A: Chem.*, 2014, **393**, 84–95; (k) E. Kolvari, N. Koukabi and O. Armandpour, *Tetrahedron*, 2014, **70**, 1383–1386.

16 (a) B. F. Mirjalili, A. Bamoniri and A. Akbari, *Tetrahedron Lett.*, 2008, **49**, 6454–6456; (b) B. F. Mirjalili, A. Bamoniri, M. A. Karimi Zarchi and H. Emtiazi, *J. Iran. Chem. Soc.*, 2010, **7**, 95–99; (c) B. F. Mirjalili, A. Bamoniri and A. Akbari, *J. Iran. Chem. Soc.*, 2011, **8**, 135–140; (d) A. Bamoniri, A. Ghorbani-Choghamarani and B. F. Mirjalili, *Phosphorus Sulfur Silicon Relat. Elem.*, 2011, **186**, 381–388; (e) A. Bamoniri, B. F. Mirjalili, A. A. Jafari and F. Abasaltian, *Iran. J. Catal.*, 2012, **2**, 73–76; (f) B. F. Mirjalili, A. Bamoniri and M. A. Mirhoseini, *Chem. Heterocycl. Compd.*, 2012, **48**, 856–860; (g) B. F. Mirjalili, A. Bamoniri and L. Zamani, *Sci. Iran.*, 2012, **19**, 565–568; (h) A. Bamoniri, B. F. Mirjalili and S. Nazemian, *Curr. Chem. Lett.*, 2013, **2**, 27–34; (i) A. Bamoniri, B. F. Mirjalili and S. Nazemian, *J. Iran. Chem. Soc.*, 2014, **11**, 653–658.

17 K. Wilson and J. H. Clark, *Chem. Commun.*, 1998, 2135–2136.

18 (a) F. Toda and K. Tanaka, *Chem. Rev.*, 2000, **100**, 1025–1074; (b) K. Tanaka, Solvent-Free Organic Synthesis, John Wiley & Sons, New York, 2003.

19 L. N. Ogoleva and B. I. Stepanov, *Ž. Org. Chim.*, 1965, **1**, 2083–2086.

20 K. J. Morgan, *J. Chem. Soc.*, 1961, 2151–2159.

21 G. Charrier and G. Ferreri, *Gazz. Chim. Ital.*, 1914, **44**, 234.

22 W. R. Brode and L. E. Herdle, *J. Org. Chem.*, 1941, **6**, 713–721.

23 E. Bamberger, *Chem. Ber.*, 1897, **30**, 513–516.

24 M. Emadi, E. Shams and M. K. Amini, *J. Chem.*, 2013, Article No. 787682, DOI:10.1155/2013/787682.

25 W. Stöber, A. Fink and E. Bohn, *J. Colloid Interface Sci.*, 1968, **26**, 62–69.

Nano-Fe_3O_4 encapsulated-silica supported boron trifluoride as a novel heterogeneous solid acid for solvent-free synthesis of arylazo-1-naphthol derivatives

Abdolhamid Bamoniri and Naimeh Moshtael-Arani

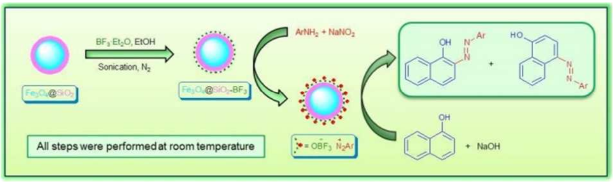

$Fe_3O_4@SiO_2-BF_3$ nanoparticles was prepared as a novel solid acid, and effectively applied for solvent-free synthesis of arylazo-1-naphthols at room temperature.